Report

Current Biology

Gamma amplitude is coupled to opposed hippocampal theta-phase states during the encoding and retrieval of episodic memories in humans

Highlights

- Hippocampal phase-amplitude coupling modulates memory in humans
- Phase preference of encoding and recall are opposed
- Theta-gamma opposition predicts memory performance

Authors

Ludovico Saint Amour di Chanaz, Alexis Pérez-Bellido, Xiongbo Wu, ..., Vincent Navarro, Antoni Valero-Cabré, Lluís Fuentemilla

Correspondence

llfuentemilla@ub.edu

In brief

Saint Amour di Chanaz et al. find evidence that hippocampal gamma is coupled to opposing theta phases during the encoding and retrieval of episodic memories. These results provide support for the memory models that involve hippocampal theta-gamma phase opposition and offer insight into similarities and differences between species.

Saint Amour di Chanaz et al., 2023, Current Biology *33*, 1836–1843
May 8, 2023
https://doi.org/10.1016/j.cub.2023.03.073

CellPress

CellPress

Current Biology

Report

Gamma amplitude is coupled to opposed hippocampal theta-phase states during the encoding and retrieval of episodic memories in humans

Ludovico Saint Amour di Chanaz,[1,2] Alexis Pérez-Bellido,[1,2] Xiongbo Wu,[1,2,3] Diego Lozano-Soldevilla,[4] Daniel Pacheco-Estefan,[5] Katia Lehongre,[6] Estefanía Conde-Blanco,[7] Pedro Roldan,[7] Claude Adam,[8] Virginie Lambrecq,[6,8,9] Valerio Frazzini,[6,8,9] Antonio Donaire,[7] Mar Carreño,[7] Vincent Navarro,[6,8,9,10] Antoni Valero-Cabré,[6,11,12,13] and Lluís Fuentemilla[1,2,14,15,*]

[1]Department of Cognition, Development and Educational Psychology, University of Barcelona, Pg Vall Hebrón 171, 08035 Barcelona, Spain
[2]Institute of Neurosciences, University of Barcelona, Pg Vall Hebrón 171, 08035 Barcelona, Spain
[3]Department of Psychology, Ludwig-Maximilians-Universität München, Munich, Germany
[4]Laboratory for Clinical Neuroscience, Centre for Biomedical Technology, Universidad Politécnica de Madrid, Crta. M40, Km. 38, Pozuelo de Alarcón, Madrid 28223, Spain
[5]Department of Neuropsychology, Institute of Cognitive Neuroscience, Faculty of Psychology, Ruhr University Bochum, 44801 Bochum, Germany
[6]Sorbonne Université, Paris Brain Institute – Institut du Cerveau, ICM, INSERM, CNRS, APHP, Pitié-Salpêtrière Hospital, 47-83, Boulevard de l'Hôpital, 75651 Paris Cedex 13, France
[7]Epilepsy Program, Neurology Department, Hospital Clínic de Barcelona, EpiCARE: European Reference Network for Epilepsy, Institut D'Investigacions Biomèdiques August Pi i Sunyer (IDIBAPS), C. de Villarroel, 170, 08036 Barcelona, Spain
[8]AP-HP, Epilepsy Unit, Pitié-Salpêtrière Hospital, DMU Neurosciences, 47-83, Boulevard de l'Hôpital, 75651 Paris Cedex 13, France
[9]AP-HP, Département de Neurophysiologie, Hôpital PitiéSalpêtrière, DMU Neurosciences, 47-83, Boulevard de l'Hôpital, 75651 Paris Cedex 13, France
[10]AP-HP, Center of Reference for Rare Epilepsies, Pitié-Salpêtrière Hospital, 47-83, Boulevard de l'Hôpital, 75651 Paris Cedex 13, France
[11]Cerebral Dynamics, Plasticity and Rehabilitation Group, FRONTLAB team, CNRS UMR 7225, INSERM U1127, Paris, France
[12]Faculty of Health and Science, Cognitive Neurolab, Neuroscience and Information Technology Research Program, Open University of Catalonia (UOC), Avinguda del Tibidabo, 39-43, 08035 Barcelona, Spain
[13]Laboratory for Cerebral Dynamics Plasticity and Rehabilitation, Boston University School of Medicine, 72 E Concord Street, Boston, MA 02118, USA
[14]Institute for Biomedical Research of Bellvitge, C/ Feixa Llarga, s/n - Pavelló de Govern -Edifici Modular, L'Hospitalet de Llobregat, 08907 Barcelona, Spain
[15]Lead contact
*Correspondence: llfuentemilla@ub.edu
https://doi.org/10.1016/j.cub.2023.03.073

SUMMARY

Computational models and *in vivo* studies in rodents suggest that the emergence of gamma activity (40–140 Hz) during memory encoding and retrieval is coupled to opposed-phase states of the underlying hippocampal theta rhythm (4–9 Hz).[1–10] However, direct evidence for whether human hippocampal gamma-modulated oscillatory activity in memory processes is coupled to opposed-phase states of the ongoing theta rhythm remains elusive. Here, we recorded local field potentials (LFPs) directly from the hippocampus of 10 patients with epilepsy, using depth electrodes. We used a memory encoding and retrieval task whereby trial unique sequences of pictures depicting real-life episodes were presented, and 24 h later, participants were asked to recall them upon the appearance of the first picture of the encoded episodic sequence. We found theta-to-gamma cross-frequency coupling that was specific to the hippocampus during both the encoding and retrieval of episodic memories. We also revealed that gamma was coupled to opposing theta phases during both encoding and recall processes. Additionally, we observed that the degree of theta-gamma phase opposition between encoding and recall was associated with participants' memory performance, so gamma power was modulated by theta phase for both remembered and forgotten trials, although only for remembered trials the dominant theta phase was different for encoding and recall trials. The current results offer direct empirical evidence in support of hippocampal theta-gamma phase opposition models in human long-term memory and provide fundamental insights into mechanistic predictions derived from computational and animal work, thereby contributing to establishing similarities and differences across species.

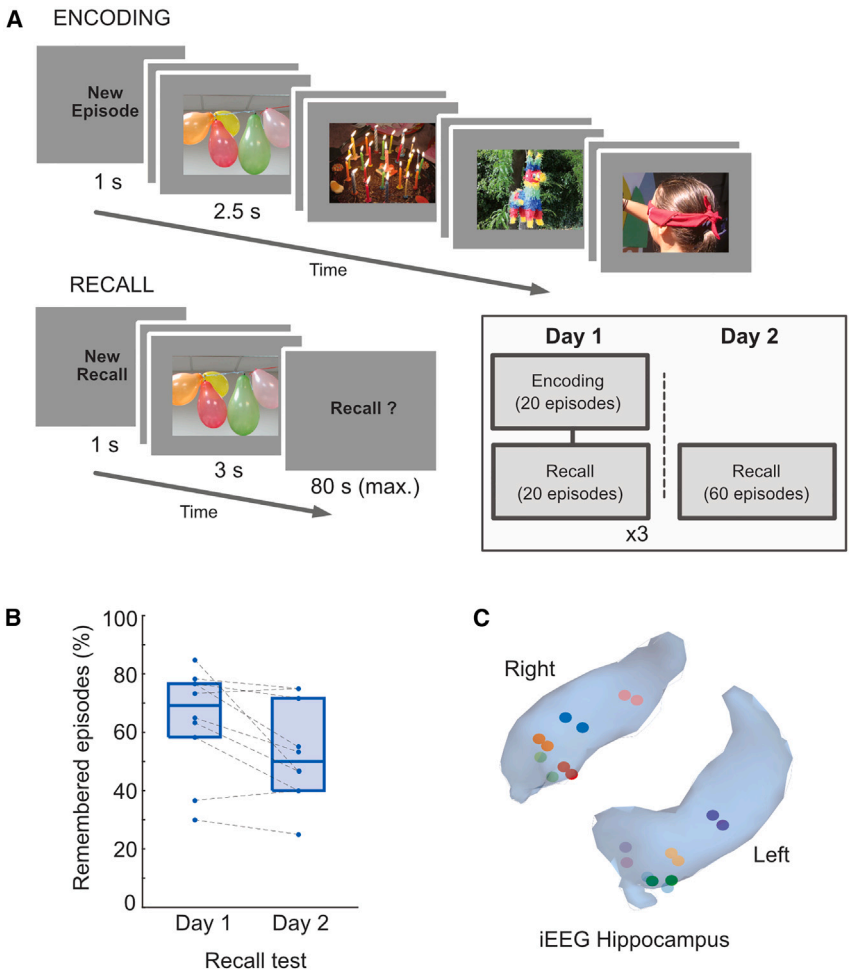

Figure 1. Experimental design and recording locations

(A) On day 1, participants were presented with 3 blocks of 20 different picture series, each including 4 pictures depicting a plausible succession of instances of a real-life episode (encoding phase). Participants were informed that memory of the encoded episodes would be tested after each encoding block on the same day (recall day 1) and again 24 h later (recall day 2). Participants were informed that the recall phase consisted of the presentation of the first picture of each of the series and that they should verbally recall the pictures associated with each of them. They were asked to be as specific and precise as possible, trying to recall the events in order and mentioning the first image as the beginning of their story.

(B) Participants' proportion of episodes that were successfully remembered in the day 1 and day 2 recall tests. In the boxplots the central mark is the median, and the edges of the box are the 25th and 75th percentiles. Each dot on both plots represents a single participant. Dashed lines on the boxplot connect the value of an individual in the two conditions.

(C) Hippocampal electrode localizations from all the participants, shown on a three-dimensional hippocampus model. Each pair of color dots indicates the two electrodes from the participants used for this study, which was used for bipolar referencing, resulting in one trace per patient.

See also Table S1.

RESULTS AND DISCUSSION

Ten participants (6 females, age 29.5 ± 11.7 years; mean ± SD) with drug-resistant epilepsy participated in a 2-day encoding and recall episodic memory task (Figure 1A). Participants studied a series of 60 different episodes of 4 picture image sequences, each depicting a plausible succession of instances of a real-life episode that they had to recall immediately (recall day 1) and then again 24 h later (recall day 2), cued with the first image of each episode. Memory accuracy was assessed by counting the number of pictures from each episode that was correctly included in the recall phase (3 being the maximum value to reach per episodic series). We then obtained a memory score for each episode that ranged from 0 (i.e., no pictures included in the recall) to 3 (i.e., all pictures included in the recall), given that the recall of the first picture was non-informative of memory retrieval as it was always displayed as a cue during the recall. The total number of recalled pictures for each episode was then used to categorize whether that episode was remembered or forgotten. We categorized episodes that included 2 or 3 pictures in their recall as "remembered," and when participants recalled 0 pictures or 1 picture from the episode, we categorized those as "forgotten." As expected, participants remembered on average more episodes in the recall task on day 1 (mean ± SD, 64.9% ± 18.1%) than in the recall task on day 2 (mean ± SD, 53.2% ± 16.5%) (paired t test, t(9) = 2.89, p = 0.02) (Figure 1B; Table S1). We also observed that the number of cases in which pictures from an episode were recalled in an incorrect order, or when these included pictures from other episodes, was infrequent in both recall day 1 (6.0% ± 4.10%) and recall day 2 (5.83% ± 2.97%) tests, and the number of errors in their recall did not differ between these two tests (t(9) = 0.16, p = 0.87), thereby indicating that participants were accurate in their remembered episodes.

While participants performed the task, we recorded direct hippocampal activity via implanted depth electrodes (Figure 1C), thereby allowing us to examine hippocampal neurophysiological mechanisms that supported episodic memory encoding and retrieval in humans. Previous work using intracranial electroencephalographic (iEEG) recordings from human hippocampus revealed increases of high-frequency gamma power (~40–120 Hz), an established correlate of firing rates of individual neurons,[11–13] increase during encoding[14] and retrieval, either in recognition[15] or in recall[16] memory tasks. We thus carried out a single-trial time-frequency analysis on hippocampal EEG data during the encoding of episodes and at their recall on day 2, and we computed the relative gamma power increases and decreases corrected with respect to a 0.5-s baseline window

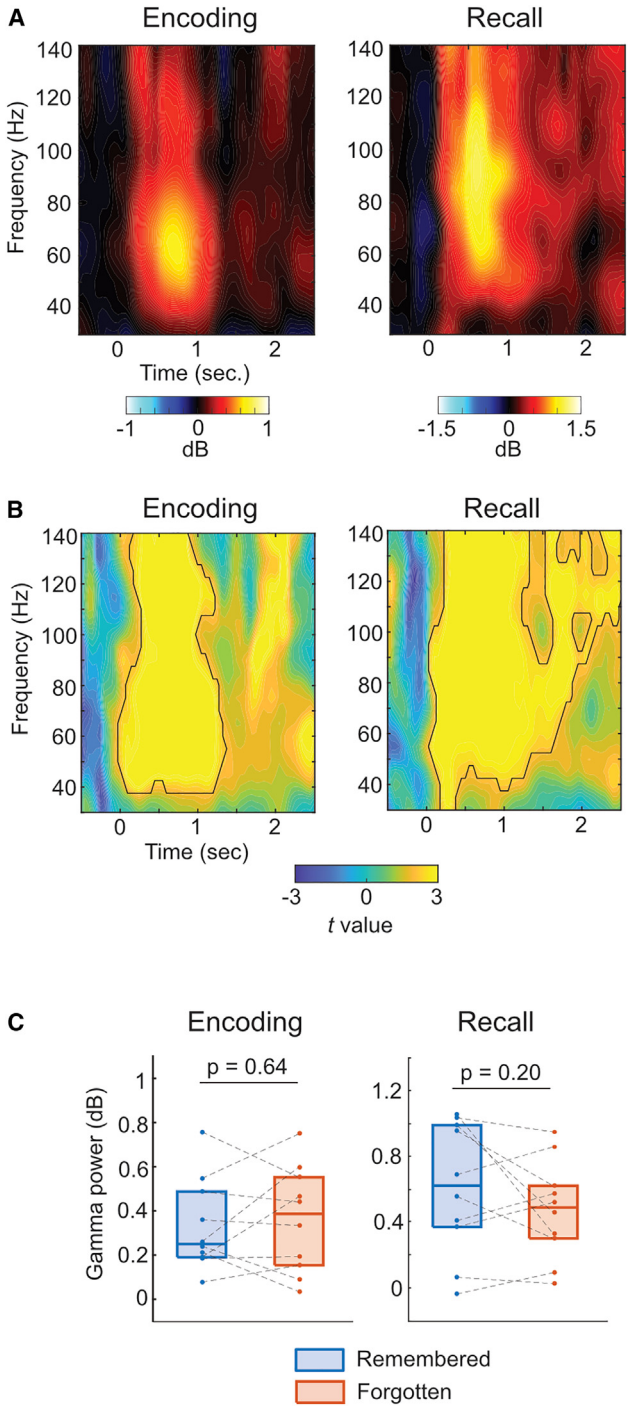

Figure 2. Hippocampal gamma power during memory encoding and recall

(A) Group-averaged changes in spectral power elicited during memory encoding and recall.

(B) Time-frequency t value map of gamma power increase and decrease at encoding and at recall. Thick black lines depict the cluster that resulted as being statistically significant at encoding and at recall ($p < 0.05$, cluster statistics).

(C) Cluster-averaged gamma power at encoding and recall for remembered and forgotten episodes. Paired t test-associated p values between conditions associated are displayed. For all boxplots, the central mark is the median, and the edges of the box are the 25th and 75th percentiles. Each dot represents the value for an individual participant in each condition. Dashed lines on the boxplots connect the value of an individual in the two conditions.

See also Figures S1, S3, and S4.

(STAR Methods). This analysis revealed that marked gamma-band (~40–140 Hz) power increase from ~0.3 to 1.3 s during memory encoding and recall (Figures 2A and S1), which proved to be statistically significant (cluster statistics at encoding, t_{sum} = 1699.1, t_{peak} = 5.97, p = 0.002; cluster statistics at recall, t_{sum} = 2503.0, t_{peak} = 6.8, p = 0.006) after correcting for multiple comparisons using a cluster-based non-parametric method (Figure 2B; STAR Methods). However, a comparison of the cluster-averaged gamma power increase for episodes that were remembered and forgotten revealed that the magnitude of the increase was similar between conditions (repeated measures ANOVA, all $F < 0.5$), both during memory encoding (paired t test: $t(9) = -0.48$, p = 0.64) and recall ($t(9) = 1.35$, p = 0.20) (Figure 2C). Additional analysis accounting for picture order within the episode confirmed that gamma power increase was consistent throughout encoding and similarly elicited by episodes that would be later remembered or forgotten (Figure S1). This contrasts with earlier findings that showed greater hippocampal gamma power response during the encoding of words from a list that were later remembered, compared with those that were forgotten,[14] or the correct identification of a color-associated background of a word during a recognition task.[15] While it would be reasonable to expect performance-dependent hippocampal gamma power modulations in our study too, there are important differences between the previous and our task design. Here, we asked participants to encode and recall the complete sequence of visual pictures depicting the unfolding of a realistic and schema-consistent episode, and we distinguished between remembered and forgotten episodes based on the participants' abilities to recollect the pictures verbally, remaining agnostic to the likely possibility that they successfully recognized the picture cues even in the forgotten trials. Thus, our task design may be less sensitive in isolating the gamma power differences between successful and unsuccessful memory performance revealed in previous studies.

We next asked whether the increase in gamma power seen during episodic encoding and during recall was coupled to the ongoing hippocampal theta-phase states. Hippocampal theta oscillations have been related to the dynamics of memory function,[17–24] and specifically to the interplay between encoding and retrieval.[1,25] In theta-based hippocampal models, the phase of ongoing theta oscillations separates encoding and retrieval and determines the different plasticity regimes that memory encoding and retrieval require.[1] Prior rodent studies reported evidence that modulations within the gamma band distinguishing encoding from retrieval,[26,27] and the study of theta on humans showed a preferential phase for encoding and recall,[28,29,30] highlighting the intrinsic property of the hippocampus to shift its dynamics toward encoding and retrieval, even when the same perceptual experience is present during the two tasks (e.g., Long et al.[31]); however, direct evidence of whether human hippocampal gamma-modulated activity in memory processes is coupled to opposed-phase states of the ongoing theta rhythm remains elusive.

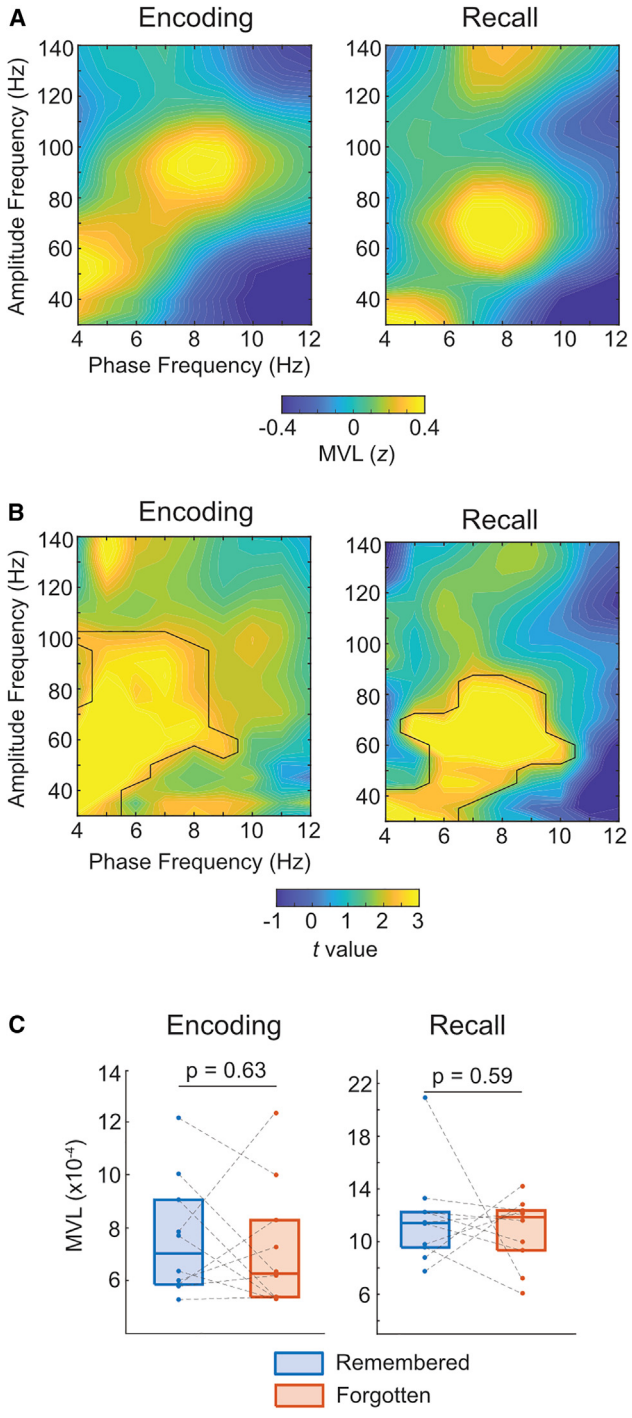

Figure 3. Hippocampal theta-gamma phase-amplitude coupling during memory encoding and recall

(A) Group-averaged phase-amplitude comodulogram computed during memory encoding and recall. x axis indicates phases modulating the signal, and the y axis represents the modulated amplitude.

(B) Phase-to-amplitude t value map during encoding and recall. Thick black lines depict the cluster that resulted statistically significant during encoding and recall ($p < 0.05$, cluster statistics).

(C) Cluster-averaged PAC strength for remembered and forgotten episodes during encoding and recall. Paired t test-associated p values between conditions associated are displayed. For all boxplots, the central mark is the median, and the edges of the box are the 25th and 75th percentiles. Each dot represents the value for an individual participant in each condition. Dashed lines on the boxplots connect the value of an individual in the two conditions. See also Figures S2–S4.

To address this issue, we first examined whether hippocampal gamma oscillations exhibited phase-amplitude coupling (PAC) with ongoing theta phase during encoding and during retrieval in our data. We assessed the existence of theta-gamma PAC by using a comodulogram method as described in Tort et al.,[32] which allows for PAC to be scanned from several narrow-filtered frequencies within the theta and gamma frequency bands. We then quantified the magnitude of PAC in each frequency pair by using the so-called mean vector length (MVL) method[33] (STAR Methods), which has been found to be relatively robust to signal-to-noise over time for EEG segments of few seconds.[34] The results of this analysis revealed that hippocampal gamma-band amplitude during memory encoding and during memory recall was modulated by the ongoing theta-phase state (Figures 3A and S2). Cluster-based statistics confirmed a statistically significant theta-gamma PAC cluster, comprising amplitude modulations in the ~40–110 Hz frequency range that were coupled to ~4–9 Hz phases during encoding (cluster statistics: $t_{sum} = 181.7$, $t_{peak} = 5.51$, $p < 0.001$) and amplitude modulations at ~50–90 Hz frequency range that were coupled to the ongoing theta phases within the ~4–10 Hz frequency range during recall (cluster statistics: $t_{sum} = 139.9$, $t_{peak} = 5.48$, $p < 0.001$) (Figure 3B). Theta-gamma PAC was also detected during recall on day 1 (i.e., in the test that took place a few minutes after encoding) (Figure S3). However, the degree of PAC between memory conditions did not differ statistically (repeated measures ANOVA, all $F < 0.3$; encoding, $t(9) = 0.49$, $p = 0.63$; recall, $t(9) = 0.54$, $p = 0.59$) (Figure 3C). Additional control analyses showed that theta oscillations were present during encoding and recall (Figure S1); that encoding theta-gamma PAC was similar throughout the sequence of encoded pictures and between memory conditions (Figure S4); that theta-gamma PAC could not be identified in other brain regions outside the hippocampus, such as in the middle temporal gyrus (Figure S4); and that the lack of theta-gamma PAC differences could not be explained by signal-to-noise properties derived from hippocampal evoked-potential responses, elicited during encoding and recall in the task (Figure S1).

The results presented thus far show that hippocampal gamma is effectively coupled to the ongoing theta-phase state, but it is not predictive of episodic memory formation and retrieval. Our analysis, however, does not account for the possibility that gamma-amplitude modulation to theta phases occurs at distinct phases at encoding and at recall, as it would be predicted by theta-phase hippocampal models.[1] To test theta phase opposition, we developed an index, the "mean opposition vector index" (MOVI), allowing us to statistically assess the existence of PAC opposition between two experimental conditions (STAR Methods). Briefly, MOVI is the MVL of an alternate distribution, calculated as the difference between the two compared distributions. Each participant had an experimental MOVI value that was tested against 1,000 surrogate values after shuffling across trials. These experimental values, as well as the surrogate values, were averaged, and we obtained an experimental MOVI value to

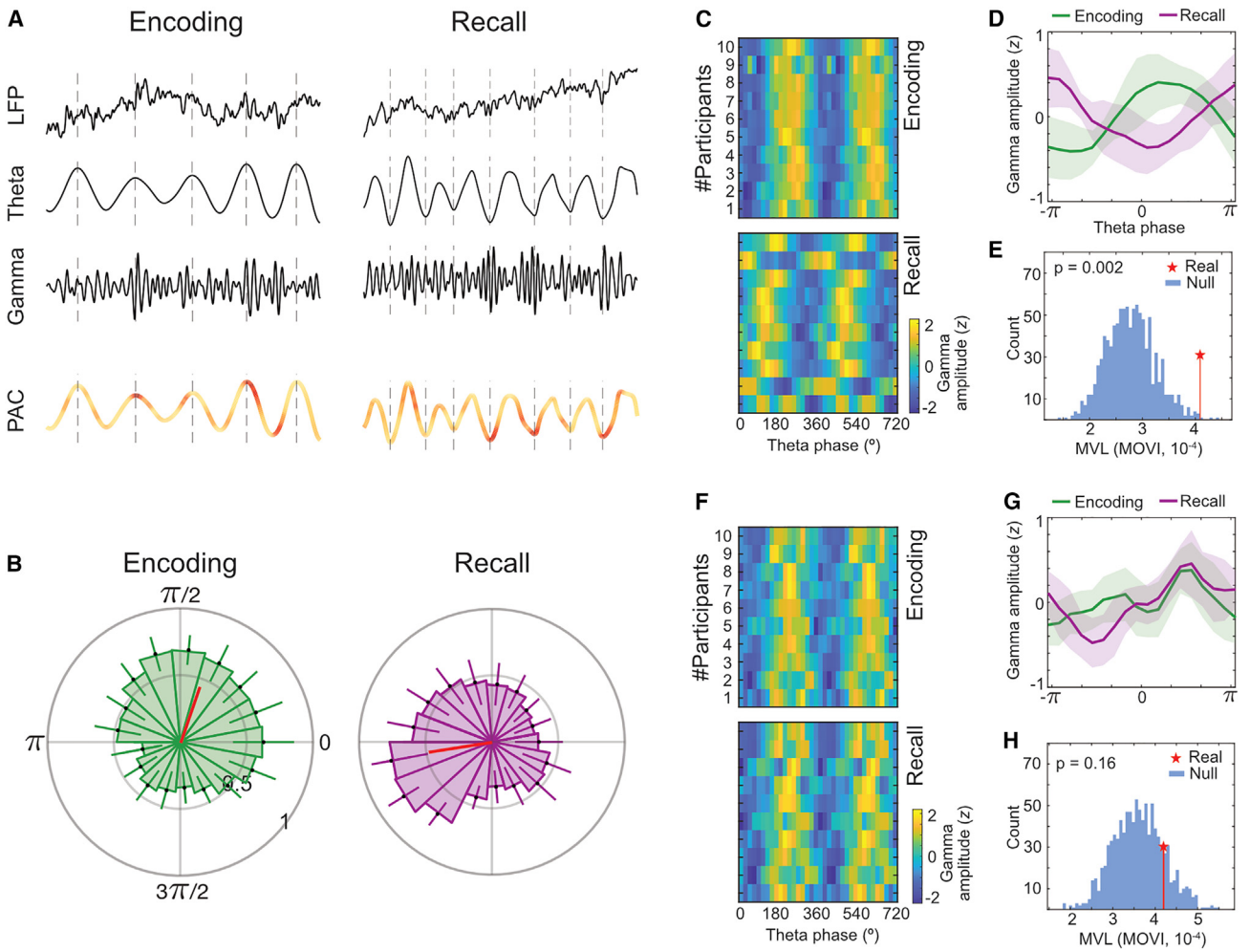

Figure 4. Hippocampal theta-gamma phase preference and mean opposition vector index (MOVI)

(A) Representative example of raw (LFP) and filtered (theta and gamma) hippocampal recordings from one of the participants of the study during encoding and at recall. The PAC wave shows where on the theta cycle there is an increase in gamma activity for the example trial.

(B) Polar distribution of averaged gamma amplitude (z) across participants over theta phases within the significant cluster of PAC found at encoding and at recall. Error bars represent standard error across participants. Grand average across participants is depicted by the thick red line.

(C) Individual distribution of hippocampal gamma amplitude over a cycle of theta at encoding and recall for remembered trials. Participants' distributions have been realigned to the mean angle direction of encoding, and the recall distributions have been realigned relative to each participant's encoding distribution for this figure only.

(D) Average distribution of hippocampal gamma amplitude over theta phase for all patients for remembered trials. Shaded area represents the SEM across participants.

(E) Experimental value of MOVI (red star) compared with surrogate value for all participants for remember trials.

(F) Individual distribution of hippocampal gamma amplitude over a cycle of theta at encoding and recall for forgotten trials. Participants' distributions have been realigned to the mean angle direction of encoding, and the recall distributions have been realigned relative to each participant's encoding distribution for this figure only.

(G) Average distribution of hippocampal gamma amplitude over theta phase for all participants for forgotten trials. Shaded area represents the standard error across participants. Note that the lack of phase preference in the plot does not reflect a lack of PAC but the degree of variability in phase preference across participants.

(H) Experimental value of MOVI (red star) compared with surrogate value for all participants for forget trials.

See also Figures S2–S4.

test against a distribution of surrogates. We *Z* scored the experimental value and obtained a p value by identifying the fraction of surrogate MOVI values that was smaller than the experimental value (STAR Methods). We found significant gamma-band activity coupling to opposed-theta-phase states during memory encoding and recall (z = 2.29, p = 0.009) (Figures 4A, 4B, and S2). This theta-gamma PAC opposition was statistically significant for remembered episodes (z = 2.85, p = 0.002) (Figures 4C and 4D) but not for forgotten episodes (z = 0.98, p = 0.16) (Figures 4E and 4F) or for the interaction remembered versus forgotten (t(9) = 0.76, p = 0.49). This result indicates that gamma power was modulated by theta phase for both

remembered and forgotten trials, although only for remembered trials the dominant theta phase was different for encoding and recall trials.

Altogether, the current study provides evidence in humans that hippocampal gamma couples to opposed-phase states of the ongoing theta rhythm activity in episodic memory during encoding and during retrieval. The present findings thus constitute empirical support for the computational models that show that the emergence of gamma oscillations at opposed-phase states of the underlying theta rhythms may be optimal for acquiring new memories and retrieving existing memories.[1,10]

While hippocampal theta-gamma PAC is well documented in task-based mnemonic processing in rodents,[2,7–10,25,35] evidence in humans has been compromised by the limited access to the direct sampling of hippocampal activity with intracranial EEG recordings. Notably though, the existing data converged in showing that hippocampal theta-phase coding scheme is a core mechanistic conduit in memory function[28,29,36,37] and that human hippocampal theta-gamma PAC underlies working memory[38,39] and the recall of list words.[40] The current findings further extend this literature by providing novel evidence that human hippocampal gamma activity functionally shifts to distinct theta-phase states to support episodic encoding or retrieval.

In line with previous studies examining memory-based hippocampal activity from intracranial recordings in humans,[15,41] we found an increase in power for a broad high-frequency range (~40–120 Hz) activity at encoding and at retrieval. Rodent research studying the dynamic interaction of the entorhinal cortex and the CA1 and CA3 subfields within the hippocampal network identified that encoding and retrieval may in fact engage two distinct gamma bands, a slow band (~30–50 Hz) and a fast band (~60–100 Hz), each of them functionally locked to different theta-phase states.[3] In this study, the size of the intracranially implanted electrodes and the rare occasions whereby the entorhinal cortex is sampled in clinical settings challenged the possibility of reliably separating slow and fast gamma activity within the entorhinal-hippocampal CA1/CA3 network in humans (but see Griffiths et al.[42] and Wang et al.[43]).

Our findings also point to the possibility that gamma coupled to a lower and a higher hippocampal theta rhythm during encoding and recall, respectively (Figure 3). Interestingly, human hippocampal theta has been reported to be slower than rodents' theta and there may be two functionally and anatomically distinct rhythms, a slower (~3 Hz) and faster (~7 Hz) theta.[44,45] We explored whether low theta was also coupled with gamma at different phases during encoding and recall, but we did not find evidence for theta phase opposition at low theta (Figure S4). A recent study in humans has shown that oscillations within the theta range varied along the longitudinal axis of the hippocampus, with theta range being slower in the anterior hippocampus and faster at the posterior hippocampus.[46] Our study, which included hippocampal activity indistinctively from electrodes located at anterior and middle hippocampal regions (Figure 1C), may have perhaps blurred together the low and high theta oscillations. Nevertheless, the extent to which low and fast theta showed different theta-gamma PAC dynamics in memory would be an interesting question to explore in future studies. Addressing this issue adequately, though, would require a rich recording sampling of the hippocampus activity along its longitudinal axis.

In sum, current findings provide new insights into the functional role of hippocampal theta-gamma cross-frequency coupling in human episodic memory. We report that gamma oscillations are coupled to the peak of the ongoing theta rhythm during memory encoding and to the trough of theta at its retrieval. Additionally, we show that the degree of theta-gamma phase opposition was associated with memory performance. Thus, our findings provide the first direct empirical evidence in support of hippocampal theta-gamma phase opposition models subtending human long-term episodic memory, bridging an important gap between existing computational, rodent, and human evidence.

STAR★METHODS

Detailed methods are provided in the online version of this paper and include the following:

- KEY RESOURCES TABLE
- RESOURCE AVAILABILITY
  - Lead contact
  - Materials availability
  - Data and code availability
- EXPERIMENTAL MODEL AND SUBJECT DETAILS
- METHOD DETAILS
  - Data collection
  - Experimental design
  - Electrode selection
  - Data preprocessing and artifact rejection
- QUANTIFICATION AND STATISTICAL ANALYSIS
  - Behavioural analysis
  - Number of iEEG trials included in the analyses
  - Hippocampal gamma power analysis
  - Phase-amplitude coupling (PAC) analyses
  - Mean Opposition Vector Index (MOVI)

SUPPLEMENTAL INFORMATION

Supplemental information can be found online at https://doi.org/10.1016/j.cub.2023.03.073.

ACKNOWLEDGMENTS

We thank Nikolai Axmacher and Benjamin Griffiths for their helpful discussions on earlier versions of the manuscript. This work was supported by the Spanish Ministerio de Ciencia, Innovación y Universidades, which is part of Agencia Estatal de Investigación (AEI), through the project PID2019-111199GB-I00 (co-funded by European Regional Development Fund; ERDF, a way to build Europe), to L.F. We thank CERCA Programme/Generalitat de Catalunya for institutional support.

AUTHOR CONTRIBUTIONS

L.S.A.d.C., A.V.-C., and L.F. designed the experiment. L.S.A.d.C., A.P.-B., X.W., and K.L. conducted the experiment. E.C.-B., P.R., C.A., V.L., K.L., V.F., A.D., M.C., and V.N. recruited and prepared patients. L.S.A.d.C., A.P.-B., X.W., D.L.-S., and D.P.-E. analyzed the data. L.S.A.d.C. and L.F. wrote the original draft. L.F. and A.P.-B. provided supervision. L.F. acquired funding.

DECLARATION OF INTERESTS

The authors declare no competing interests.

INCLUSION AND DIVERSITY

We support inclusive, diverse, and equitable conduct of research.

Received: October 7, 2022
Revised: January 5, 2023
Accepted: March 24, 2023
Published: April 14, 2023

REFERENCES

1. Hasselmo, M.E., Bodelón, C., and Wyble, B.P. (2002). A proposed function for hippocampal theta rhythm: separate phases of encoding and retrieval enhance reversal of prior learning. Neural Comput. *14*, 793–817.
2. Manns, J.R., Zilli, E.A., Ong, K.C., Hasselmo, M.E., and Eichenbaum, H. (2007). Hippocampal CA1 spiking during encoding and retrieval: relation to theta phase. Neurobiol. Learn. Mem. *87*, 9–20.
3. Colgin, L.L., Denninger, T., Fyhn, M., Hafting, T., Bonnevie, T., Jensen, O., Moser, M.B., and Moser, E.I. (2009). Frequency of gamma oscillations routes flow of information in the hippocampus. Nature *462*, 353–357.
4. Bieri, K.W., Bobbitt, K.N., and Colgin, L.L. (2014). Slow and fast gamma rhythms coordinate different spatial coding modes in hippocampal place cells. Neuron *82*, 670–681.
5. Fernández-Ruiz, A., Oliva, A., Nagy, G.A., Maurer, A.P., Berényi, A., and Buzsáki, G. (2017). Entorhinal-CA3 dual-input control of spike timing in the hippocampus by theta gamma coupling. Neuron *93*, 1213–1226.e5.
6. Amemiya, S., and Redish, A.D. (2018). Hippocampal theta-gamma coupling reflects state-dependent information processing in decision making. Cell Rep. *22*, 3328–3338.
7. Douchamps, V., Jeewajee, A., Blundell, P., Burgess, N., and Lever, C. (2013). Evidence for encoding versus retrieval scheduling in the hippocampus by theta phase and acetylcholine. J. Neurosci. *33*, 8689–8704.
8. Lever, C., Burton, S., Jeewajee, A., Wills, T.J., Cacucci, F., Burgess, N., and O'Keefe, J. (2010). Environmental novelty elicits a later theta phase of firing in CA1 but not subiculum. Hippocampus *20*, 229–234.
9. Poulter, S., Lee, S.A., Dachtler, J., Wills, T.J., and Lever, C. (2021). Vector trace cells in the subiculum of the hippocampal formation. Nat. Neurosci. *24*, 266–275.
10. Hasselmo, M.E., and Stern, C.E. (2014). Theta rhythm and the encoding and retrieval of space and time. Neuroimage *85*, 656–666.
11. Jacobs, J., Kahana, M.J., Ekstrom, A.D., and Fried, I. (2007). Brain oscillations control timing of single-neuron activity in humans. J. Neurosci. *27*, 3839–3844.
12. Hirabayashi, T., Tamura, K., Takeuchi, D., Takeda, M., Koyano, K.W., and Miyashita, Y. (2014). Distinct neuronal interactions in anterior inferotemporal areas of macaque monkeys during retrieval of object association memory. J. Neurosci. *34*, 9377–9388.
13. Manning, J.R., Jacobs, J., Fried, I., and Kahana, M.J. (2009). Broadband shifts in local field potential power spectra are correlated with single-neuron spiking in humans. J. Neurosci. *29*, 13613–13620.
14. Sederberg, P.B., Schulze-Bonhage, A., Madsen, J.R., Bromfield, E.B., Litt, B., Brandt, A., and Kahana, M.J. (2007). Gamma oscillations distinguish true from false memories. Psychol. Sci. *18*, 927–932.
15. Staresina, B.P., Michelmann, S., Bonnefond, M., Jensen, O., Axmacher, N., and Fell, J. (2016). Hippocampal pattern completion is linked to gamma power increases and alpha power decreases during recollection. eLife *5*, e17397.
16. Burke, J.F., Sharan, A.D., Sperling, M.R., Ramayya, A.G., Evans, J.J., Healey, M.K., Beck, E.N., Davis, K.A., Lucas, T.H., and Kahana, M.J. (2014). Theta and high-frequency activity mark spontaneous recall of episodic memories. J. Neurosci. *34*, 11355–11365.
17. O'Keefe, J., and Nadel, L. (1978). The Hippocampus as a Cognitive Map (Oxford University Press).
18. Jones, M.W., and Wilson, M.A. (2005). Theta rhythms coordinate hippocampal-prefrontal interactions in a spatial memory task. PLoS Biol. *3*, e402.
19. Huxter, J.R., Senior, T.J., Allen, K., and Csicsvari, J. (2008). Theta phase-specific codes for two-dimensional position, trajectory and heading in the hippocampus. Nat. Neurosci. *11*, 587–594.
20. Buzsáki, G. (2002). Theta oscillations in the hippocampus. Neuron *33*, 325–340.
21. Tort, A.B., Komorowski, R.W., Manns, J.R., Kopell, N.J., and Eichenbaum, H. (2009). Theta–gamma coupling increases during the learning of item–context associations. Proc. Natl. Acad. Sci. USA *106*, 20942–20947.
22. Jezek, K., Henriksen, E.J., Treves, A., Moser, E.I., and Moser, M.B. (2011). Theta-paced flickering between place-cell maps in the hippocampus. Nature *478*, 246–249.
23. Kunz, L., Wang, L., Lachner-Piza, D., Zhang, H., Brandt, A., Dümpelmann, M., Reinacher, P.C., Coenen, V.A., Chen, D., Wang, W.X., et al. (2019). Hippocampal theta phases organize the reactivation of large-scale electrophysiological representations during goal-directed navigation. Sci. Adv. *5*, eaav8192.
24. Reddy, L., Self, M.W., Zoefel, B., Poncet, M., Possel, J.K., Peters, J.C., Baayen, J.C., Idema, S., VanRullen, R., and Roelfsema, P.R. (2021). Theta-phase dependent neuronal coding during sequence learning in human single neurons. Nat. Commun. *12*, 4839.
25. Kunec, S., Hasselmo, M.E., and Kopell, N. (2005). Encoding and retrieval in the CA3 region of the hippocampus: a model of theta-phase separation. J. Neurophysiol. *94*, 70–82.
26. Bragin, A., Jandó, G., Nádasdy, Z., Hetke, J., Wise, K., and Buzsáki, G. (1995). Gamma (40–100 Hz) oscillation in the hippocampus of the behaving rat. J. Neurosci. *15*, 47–60.
27. Colgin, L.L. (2015). Theta-gamma coupling in the entorhinal-hippocampal system. Curr. Opin. Neurobiol. *31*, 45–50.
28. Rizzuto, D.S., Madsen, J.R., Bromfield, E.B., Schulze-Bonhage, A., and Kahana, M.J. (2006). Human neocortical oscillations exhibit theta phase differences between encoding and retrieval. Neuroimage *31*, 1352–1358.
29. Ter Wal, M., Linde-Domingo, J., Lifanov, J., Roux, F., Kolibius, L.D., Gollwitzer, S., Lang, J., Hamer, H., Rollings, D., Sawlani, V., et al. (2021). Theta rhythmicity governs human behavior and hippocampal signals during memory-dependent tasks. Nat. Commun. *12*, 7048.
30. Kerrén, C., Linde-Domingo, J., Hanslmayr, S., and Wimber, M. (2018). An optimal oscillatory phase for pattern reactivation during memory retrieval. Curr. Biol. *28*, 3383–3392.e6.
31. Long, N.M., and Kuhl, B.A. (2021). Cortical representations of visual stimuli shift locations with changes in memory states. Curr. Biol. *31*, 1119–1126.e5.
32. Tort, A.B., Kramer, M.A., Thorn, C., Gibson, D.J., Kubota, Y., Graybiel, A.M., and Kopell, N.J. (2008). Dynamic cross-frequency couplings of local field potential oscillations in rat striatum and hippocampus during performance of a T-maze task. Proc. Natl. Acad. Sci. USA *105*, 20517–20522.
33. Canolty, R.T., Edwards, E., Dalal, S.S., Soltani, M., Nagarajan, S.S., Kirsch, H.E., Berger, M.S., Barbaro, N.M., and Knight, R.T. (2006). High gamma power is phase-locked to the theta oscillations in human neocortex. Science *313*, 1626–1628.
34. Tort, A.B., Komorowski, R., Eichenbaum, H., and Kopell, N. (2010). Measuring phase-amplitude coupling between neuronal oscillations of different frequencies. J. Neurophysiol. *104*, 1195–1210.
35. Siegle, J.H., and Wilson, M.A. (2014). Enhancement of encoding and retrieval functions through theta phase-specific manipulation of hippocampus. eLife *29*, e03061.
36. Solomon, E.A., Lega, B.C., Sperling, M.R., and Kahana, M.J. (2019). Hippocampal theta codes for distances in semantic and temporal spaces. Proc. Natl. Acad. Sci. USA *116*, 24343–24352.

37. Pacheco Estefan, D., Zucca, R., Arsiwalla, X., Principe, A., Zhang, H., Rocamora, R., Axmacher, N., and Verschure, P.F.M.J. (2021). Volitional learning promotes theta phase coding in the human hippocampus. Proc. Natl. Acad. Sci. USA *118*. e2021238118.

38. Bahramisharif, A., Jensen, O., Jacobs, J., and Lisman, J. (2018). Serial representation of items during working memory maintenance at letter-selective cortical sites. PLoS Biol. *16*, e2003805.

39. Axmacher, N., Henseler, M.M., Jensen, O., Weinreich, I., Elger, C.E., and Fell, J. (2010). Cross-frequency coupling supports multi-item working memory in the human hippocampus. Proc. Natl. Acad. Sci. USA *107*, 3228–3233.

40. Lega, B., Burke, J., Jacobs, J., and Kahana, M.J. (2016). Slow-theta-to-gamma phase–amplitude coupling in human hippocampus supports the formation of new episodic memories. Cereb. Cortex *26*, 268–278.

41. Lohnas, L.J., Duncan, K., Doyle, W.K., Thesen, T., Devinsky, O., and Davachi, L. (2018). Time-resolved neural reinstatement and pattern separation during memory decisions in human hippocampus. Proc. Natl. Acad. Sci. USA *115*, E7418–E7427.

42. Griffiths, B.J., Parish, G., Roux, F., Michelmann, S., van der Plas, M., Kolibius, L.D., Chelvarajah, R., Rollings, D.T., Sawlani, V., Hamer, H., et al. (2019). Directional coupling of slow and fast hippocampal gamma with neocortical alpha/beta oscillations in human episodic memory. Proc. Natl. Acad. Sci. USA *116*, 21834–21842.

43. Wang, D.X., Schmitt, K., Seger, S., Davila, C.E., and Lega, B.C. (2021). Cross-regional phase amplitude coupling supports the encoding of episodic memories. Hippocampus *31*, 481–492.

44. Jacobs, J. (2013). Hippocampal theta oscillations are slower in humans than in rodents: implications for models of spatial navigation and memory. Philos. Trans. R. Soc. Lond. B Biol. Sci. *369*, 20130304.

45. Lega, B.C., Jacobs, J., and Kahana, M. (2012). Human hippocampal theta oscillations and the formation of episodic memories. Hippocampus *22*, 748–761.

46. Goyal, A., Miller, J., Qasim, S.E., Watrous, A.J., Zhang, H., Stein, J.M., Inman, C.S., Gross, R.E., Willie, J.T., Lega, B., et al. (2020). Functionally distinct high and low theta oscillations in the human hippocampus. Nat. Commun. *11*, 2469.

47. Brainard, D.H. (1997). The psychophysics toolbox. Spat. Vis. *10*, 433–436.

48. Michelmann, S., Treder, M.S., Griffiths, B., Kerrén, C., Roux, F., Wimber, M., Rollings, D., Sawlani, V., Chelvarajah, R., Gollwitzer, S., et al. (2018). Data-driven re-referencing of intracranial EEG based on independent component analysis (ICA). J. Neurosci. Methods *307*, 125–137.

49. Oostenveld, R., Fries, P., Maris, E., and Schoffelen, J.M. (2011). FieldTrip: open source software for advanced analysis of MEG, EEG, and invasive electrophysiological data. Comput. Intell. Neurosci. *2011*, 156869.

50. Maris, E., and Oostenveld, R. (2007). Nonparametric statistical testing of EEG- and MEG-data. J. Neurosci. Methods *164*, 177–190.

51. Delorme, A., and Makeig, S. (2004). EEGLAB: an open source toolbox for analysis of single-trial EEG dynamics including independent component analysis. J. Neurosci. Methods *134*, 9–21.

52. Aru, J., Aru, J., Priesemann, V., Wibral, M., Lana, L., Pipa, G., Singer, W., and Vicente, R. (2015). Untangling cross-frequency coupling in neuroscience. Curr. Opin. Neurobiol. *31*, 51–61.

53. Staresina, B.P., Bergmann, T.O., Bonnefond, M., van der Meij, R., Jensen, O., Deuker, L., Elger, C.E., Axmacher, N., and Fell, J. (2015). Hierarchical nesting of slow oscillations, spindles and ripples in the human hippocampus during sleep. Nat. Neurosci. *18*, 1679–1686.

54. Heusser, A.C., Poeppel, D., Ezzyat, Y., and Davachi, L. (2016). Episodic sequence memory is supported by a theta-gamma phase code. Nat. Neurosci. *19*, 1374–1380.

55. Nielsen, F. (2019). On the Jensen-Shannon symmetrization of distances relying on abstract means. Entropy (Basel) *21*, 485.

56. VanRullen, R. (2016). How to evaluate phase differences between trial groups in ongoing electrophysiological signals. Front. Neurosci. *10*, 426.

57. Berens, P. (2009). CircStat: a MATLAB toolbox for circular statistics. J. Stat. Software *31*, 1–21.

58. Vinck, M., van Wingerden, M., Womelsdorf, T., Fries, P., and Pennartz, C.M. (2010). The pairwise phase consistency: a bias-free measure of rhythmic neuronal synchronization. Neuroimage *51*, 112–122.

STAR★METHODS

KEY RESOURCES TABLE

REAGENT or RESOURCE	SOURCE	IDENTIFIER
Software and algorithms		
MATLAB	https://uk.mathworks.com/products/matlab.html	2021a
PsychToolbox3.0	http://psychtoolbox.org/	2017
FieldTrip Toolbox	https://www.fieldtriptoolbox.org/	v.06/02/2017 v.12/05/2020
CircStat Toolbox	https://www.jstatsoft.org/article/view/v031i10	N/A
EEGLab Toolbox	https://sccn.ucsd.edu/eeglab/index.php	2019.1
Freesurfer Toolbox	https://surfer.nmr.mgh.harvard.edu/	V6
SPM12 ToolBox	https://www.fil.ion.ucl.ac.uk/spm/software/spm12/	N/A
Permutest function	https://uk.mathworks.com/matlabcentral/fileexchange/71737-permutest?requestedDomain=	1.0.0
Experiment Code	https://github.com/DMFresearchlab/OppositionPhase/tree/main/Scripts	N/A
Analysis Code	https://github.com/DMFresearchlab/OppositionPhase/tree/main/ScriptsReviewPaper	N/A
Other		
Experiment material	https://github.com/DMFresearchlab/OppositionPhase/tree/main/ImagesForTask	N/A

RESOURCE AVAILABILITY

Lead contact

For further information or requests, contact should be directed towards the lead contact, Lluís Fuentemilla (llfuentemilla@ub.edu).

Materials availability

This study did not generate new, unique reagents or materials. New analysis techniques are part of the code supplied in the data and code availability section.

Data and code availability

- The data reported in this study cannot be deposited in a public repository as it countervails to a legal prohibition (the data are confidential medical records).
- Experimental material for the cognitive task has been deposited on an open repository on GitHub (GitHub: https://github.com/DMFresearchlab/OppositionPhase/tree/main/ImagesForTask) and is publicly available as of the date of publication.
- All original code has been deposited on an open repository on GitHub (https://github.com/DMFresearchlab/OppositionPhase/tree/main/ScriptsReviewPaper) and is publicly available as of the date of publication.

EXPERIMENTAL MODEL AND SUBJECT DETAILS

Ten epilepsy patients (6 females, age 29.5 ± 11.7 years - mean ± SD) implanted with depth electrodes as part of their diagnostic assessment for pharmaco-resistant focal epilepsy participated in our study. Recordings were performed in two hospitals: the Hôpital Pitié-Salpétrière in Paris (France) and the Hospital Clínic - IDIBAPS in Barcelona (Spain). Electrode placement was exclusively guided by the clinical needs of localizing the seizure onset zone and consider the indications and feasibility of ulterior surgical resections. Participant selection was based on the following inclusion criteria: 1) normal IQ; 2) electrodes implanted in the hippocampus contralateral to or outside of the epileptogenic region were included for the analysis of neurophysiology signals. The study was conducted according to the Declaration of Helsinki and approved by the local ethics committee, and all patients provided written informed consent.

METHOD DETAILS

Data collection

The experiment was conducted in a sound-attenuated room in the hospital, with participants sitting upright in a comfortable chair or on their bed. The stimuli were presented on a 13-inch portable computer, placed on an overbed table at approximately 60 cm distance in front of the patients. Patients used the keyboard of the laptop to complete the behavioral task, and their responses were recorded. Trial onsets and offsets TTL triggers were sent to the EEG amplifier via a parallel port or an Arduino simulating a parallel port. In Paris, the recordings were performed using the ATLAS amplifier (Atlas, Neuralynx, Bozeman, MO; 160 channels at 4096 Hz; bandpass filter between 0.1 Hz and 1000 Hz). The macroelectrodes (AdTech, Wisconsin) used consisted of 4-12 platinum contact electrodes with a diameter of 1.12 mm and length of 2.41 mm, with nickel-chromium wiring. The distance between the centre of 2 contacts was 5 mm. In Barcelona the recordings were performed using a clinical EEG system (Natus Quantum LTM Amplifier) with a 1024Hz sampling rate and an online bandpass filter from 0.1Hz to 4000Hz. Intracerebral electrodes (Microdeep, DIXI Medical) were used for recordings. Each multielectrode had 8 to 18 contacts, spaced 5 mm and 1 to 2 mm long with a diameter of 0.8 mm. Verbal recalls were recorded with an audio recorder placed on the overbed table next to the laptop computer used to record responses.

Experimental design

The experiment was conducted on two consecutive days (Figure 1A). On day 1, participants were presented with 3 blocks of 20 different episodic sequences each including 4 pictures depicting a plausible succession of instances of a real-life episode (encoding phase). Participants were instructed to encode the temporally extended episodes, whereby each single-exposure episode was itself composed of four discrete and unique picture stimuli assembled into an unfolding episode. They were also informed that their memory of each of the pictures within the episodes would be tested briefly after each encoding block (recall day 1) on the same day and again 24h later (recall day 2).

In the encoding phase, participants were presented with a total of 60 different episodic sequences separated into 3 different blocks. Each episode included 4 different pictures presented sequentially. The trial structure was as follows: each trial started with the text presentation of "New Episode" for 1 s which marked the start of a new encoding episode. Each picture was then sequentially presented on a grey screen for 2.5 s and preceded by a black fixation cross in the centre of the screen for 1 s. A fixation cross was displayed again for 2 s after the 4th picture, after which participants were instructed to rate, on a keyboard (keys 1, 2, 3 and 4), how much the sequence was emotionally salient to them. The emotional salience had to be rated on a scale from 1 (no salience or boring) to 4 (very salient). An inter-trial interval of 2 s was inserted before the start of the next encoding trial.

After each encoding block of 20 episodes, participants had a short break and started the recall phase (day 1). Participants were informed that the recall phase consisted of the presentation of the first picture of each of the series and that they should verbally recall the pictures associated with each of them. They were asked to be as specific and precise as possible, and to try to recall the pictures in the exact same order as they were presented, and to mention the first image as the beginning of their recall. Patients answered in their native language which was French in the Hôpital Pitié-Salpétrière in Paris and Spanish or Catalan in the Hospital Clínic – IDIBAPS in Barcelona. Each recall trial event began with a 1 sec text presentation on the screen that depicted "New memory". After a black fixation cross in the centre of the screen for 1 s, the first picture of one of the encoded episodes was presented for 3 s, serving as a cue to prompt the verbal recall of the rest of the pictures in that episodic sequence. Participants were instructed to withhold their recall of the associated episode until the picture image was replaced by a message saying, "Can you recall the episode?", which lasted a maximum of 80 s to allow them to take their time to recall the episode if needed. An external recorder positioned on the table adjacent to the laptop was used to record their verbal responses; however, since it was not connected to the laptop, the reaction times for the answers were not obtainable. Participants could press the spacebar to end the trial when they had finished the recall. Participants were instructed beforehand to explicitly say "I do not remember" after the picture image disappeared if nothing could be remembered that was associated with the picture cue. A short break of 5-10 minutes separated the start of the new encoding-recall block.

On day 2, participants were instructed that the cued recall task would be repeated (recall on day 2) and it would follow the same trial structure as in the recall phase on day 1. All 60 first pictures from the encoded series were presented in blocks of 20 trials, which were separated by a short 5-10 minutes break.

The presentation order of the series in the encoding phase was randomized for each participant and presented in a shuffled order on each round of recall on day 1. The order of the presentation of the picture cues from the 60 episodes was also shuffled for each participant. The task was programmed on Matlab R2017b using the Psychtoolbox3 toolbox.[47]

Electrode selection

Based on anatomical and functional criteria, one pair of hippocampal depth electrode contacts per participant was selected for analyses. Depth electrodes were implanted stereotaxically, and laterally via the temporal lobe. The presence of electrodes in the hippocampus was assessed with the examination of a computed tomography (CT) and (post-electrode removal) Magnetic Resonance Imaging (MRI) T1 scans. Cerebral atlases of each patient were obtained with the parcellation of the preoperatory T1 using Freesurfer (https://surfer.nmr.mgh.harvard.edu). The CT was then co-registered to the T1 and contact tags and names were placed manually using fieldtrip toolbox for ECoG and sEEG recordings (https://www.fieldtriptoolbox.org/). Confirmation of contact placement was then obtained with a co-registration of the post-operatory T1 to the preoperatory T1 and via superposition of the electrode placement

matrix to the realigned post-operatory T1, and manual correction of the misplaced contact tags. Selection of channels was done in native space to prevent errors due to distortions while converting in MNI space. MNI space conversion was then done to have a generalized view of the patient's channels of interest. Since channels were referenced to the adjacent more distal contact along the electrode (bipolar referencing) channels of interest were selected on the bases of three main criteria (in this order of decreasing importance): (1) the channel of interest or the referenced one had to be in the hippocampus; (2) if more than one channel was eligible, hence fulfilled the prior criterion, to avoid using white matter references, hence limit noise from other brain areas, we privileged the channel that had an adjacent distal referencing contact also in the hippocampus[48]; Finally, (3) if more than one pair of adjacent channels were eligible, we selected those that had the least amount of epileptic activity according to the Artifact Rejection procedure (please see section below for details).

To visualize the selected contacts across our sample, we normalized each participant's post-implantation MRI along with their co-registered pre-implantation MRI to MNI space using SPM12 (http://www.fil.ion.ucl.ac.uk/spm/). To facilitate the visualization of contacts across the group, a 5-mm-radius sphere was created around each contact's centre point and overlaid across participants (Figure 1C).

Data preprocessing and artifact rejection

We first down-sampled raw EEG data from all participants to 1000 Hz. Then, we extracted epochs of EEG data from -2 to +4 s from stimulus onset for all stimuli (picture images) and plotted each EEG trial data to perform a visual inspection to identify epileptic activity with the help of an epileptologist. We recognized interictal spikes and epileptic activity, characterized by high amplitude EEG signals that were disruptive of previously ongoing activity. We then plotted each trial's spectral power (30 – 140 Hz) to evaluate the presence of noise in the time-frequency domain. Trials containing epileptic activity or noise were removed from further analysis. This resulted in 47.8 ± 10.8 (Mean ± SD) trials for image 1, 48.5 ± 10.8 trials for image 2, 49.6 ± 8.3 trials for image 3, 50.8 ± 8.3 trials for image 4 and 52.9 ± 10.0 trials for recall, being kept for analysis on average across patients, for a total of 60 trials per stimulus. We then re-referenced each contact to the closest contact on the same electrode (bipolar re-referencing, details explained above) and performed a second visual inspection of the LFPs and the spectral power data to ensure all epileptic spikes had been successfully removed throughout our priori Artifact Rejection procedure.

QUANTIFICATION AND STATISTICAL ANALYSIS

Behavioural analysis

Participants' memory accuracy was assessed by analysing the verbal recall on day 1 and day 2. For each episode, each picture was counted as remembered or forgotten. A picture was counted as remembered when participants mentioned an action or an item that clearly depicted the content of the picture. We then obtained a memory score for each episode that ranged from 0 (i.e., no pictures included in the recall) to 3 (i.e., all pictures were included in the recall), given that the recall of the first picture was non-informative of memory retrieval as it was always displayed as a cue during the recall. The total number of pictures correctly recalled for each episode was then used to categorize whether that episode was remembered or forgotten. We categorized episodes that included 2 or 3 correctly recalled pictures as 'remembered' and 'forgotten' when participants recalled either none or a single picture from the episode. When pictures were correctly recalled in an episode, we also assigned a number from 2 to 4 to each of them to index the correspondence to the order position in the sequence at encoding. This allowed us assessing for the possibility that remembered pictures were recalled in an incorrect order during the recall (e.g., permutation errors). We also coded if pictures from one encoded episode were erroneously recalled in another one at test (e.g., false alarms).

To evaluate the extent to which recalled episodes in the immediate test were consistent to those recalled in the delayed test, we performed a linear regression analysis at the individual level using the number of pictures recalled in the immediate test as a dependent variable and the number of pictures recalled in the delayed test as an independent measure. If the pictures recalled in the delay recall test from each of the episodes scaled according to the recalled pictures at the immediate test, then the slope of this relationship should be positive and differ from 0. This analysis revealed that this was the case, as the slopes were positive (mean ± SD, 0.73 ± 0.16) and significantly above 0 ($t(9) = 14.62$, $p < 0.001$). These results indicate that the number of recalled images per episode was consistent in the recall test on day 1 and on day 2.

On average, participants rated the encoded episodes as emotionally neutral (mean ± SD, 2.46 ± 0.69; Participant 9 had to be excluded from this analysis because of with the recording of button presses during the encoding phase). Ratings were similar for remembered and forgotten episodes as a function of memory accuracy in the immediate (remembered: 2.49 ± 0.73 and forgotten: 2.46 ± 0.68, paired t-test $t(8) = 0.18$, $p = 0.86$) and in delayed recall test (remembered: 2.47 ± 0.78 and forgotten: 2.46 ± 0.59, paired t-test $t(8) = 0.05$, $p = 0.96$). These results indicate that participants' episodic engagement did not affect successful memory accuracy in our experiment.

Number of iEEG trials included in the analyses

We quantified the number of trials from each of the 4 pictures at encoding and at recall that were included in the iEEG analyses after artifact rejection and have them compared across memory conditions for each of the recall tests. We statistically assessed this issue at encoding by running a repeated measures ANOVA including two within-subject factors, memory type (remembered, forgotten) and picture position (1^{st}, 2^{nd}, 3^{rd}, 4^{th} in the episodic sequence). We used a paired-t test at recall as a statistical test for this issue.

This statistical approach revealed that the number of iEEG trials included in the analysis of the immediate recall test was, as expected, greater in the 'remembered' than in the 'forgotten' condition (repeated measures ANOVA, main effect of memory $F(1,9) = 5.25$, $p = 0.048$). This analysis also showed a statistically significant memory × picture position interaction ($F(3,27) = 3.81$, $p = 0.02$; but not a main picture position effect $F(3,27) = 0.84$, $p = 0.48$), which indicated that the difference in the number of iEEG trials between conditions was not homogeneous throughout the picture sequence. Similarly, a paired t-test confirmed there were more trials in the 'remembered' than in the 'forgotten' conditions during the recall phase ($t(9) = 2.71$, $p = 0.02$). For completeness, we detailed the number of trials in the immediate recall test: 'remembered' condition: 29.7 ± 10.5 for image 1, 31 ± 12.4 for image 2, 32.2 ± 10.4 for image 3, 32.6 ± 11.5 for image 4 and 35.6 ± 9.66 for the recall phase. The number of trials included in the 'forgotten' condition was 18.1 ± 11 for image 1, 17.5 ± 5 for image 2, 17.4 ± 9.9 for image 3, 18.2 ± 9.2 for image 4 and 19.1 ± 10.01 for the recall phase.

However, the number of iEEG trials included in the analysis in the remembered and forgotten condition in the delay recall test showed to be not statistically different (repeated measures ANOVA: main effect of memory $F(1,9) = 0.39$, $p = 0.55$; main effect of picture order $F(3,27) = 0.84$, $p = 0.48$; interaction memory × picture order $F(3,27) = 0.71$, $p = 0.55$). Similarly, the number of trials included in the iEEG analysis was equivalent in the recall phase for the remember and forget conditions ($t(9) = 0.81$, $p = 0.44$). For completeness, here we detail the number of iEEG trials in each condition for the delayed recall test: 'remembered' condition: 25.5 ± 11.5 for image 1, 22.3 ± 10.1 for image 2, 27 ± 11 for image 3, 27.4 ± 11.7 for image 4 and 28.9 ± 11.42 for the delayed recall phase. The number of trials included in the 'forgotten' condition was 22.3 ± 10.1 for image 1, 22.7 ± 8.7 for image 2, 22.6 ± 9.1 for image 3, 23.4 ± 8.6 for image 4 and 24 ± 10.16 for the delayed recall phase.

These results are important as they ensure that the iEEG findings reported in the current study, which compared hippocampus iEEG signals for encoding and delay recall phases, cannot be simply explained by the difference in the number of analysed trials between the remembered and forgotten conditions.

Hippocampal gamma power analysis

Data analysis of spectral power was performed using Fieldtrip[40] and standard MATLAB functions on the 6 s iEEG epochs selected during the preprocessing stage. The 6 s time window included -2 s from picture onset to avoid padding on low frequencies in the targeted smaller temporal window of 2.5 s from picture onset in subsequent analysis. Frequency decomposition of the data was performed via Fourier analysis based on sliding time windows (moving forward in 10 ms increments). We applied a multi-tapering procedure and a DPSS filter with a fixed window length of 500 ms and seven orthogonal Slepian tapers, resulting in a spectral smoothing of ∼ ± 10 Hz. The resulting power maps were decibel corrected with the average of the -0.5 s prestimulus baseline. For statistical analysis of power maps, we used a non-parametric cluster-based permutation procedure implemented in FieldTrip[49] and searched for power fluctuations against artificial data created by time-shuffling the experimental data. We tested the experimental data against the time-shuffled data in a cluster-based permutation test where labels of the experimental and artificial data were randomly shuffled across participants 1000 times without repetition of combinations. The alpha level was set to 5% across analyses, and parametric t-tests were two-tailed.[50] Spectral power (but also PAC and MOVI described below) was studied within a window of 2.5 s from picture onset. During encoding, the 2.5 s corresponded to the time window of each of the pictures in the sequence and, during recall, this time window corresponded to the time window where the cue picture was on the screen. This way, the results at encoding and recall could be comparable in terms of temporal signal-to-noise properties of the iEEG signal and frequency resolution of the analyses.

Phase-amplitude coupling (PAC) analyses

For the identification of PAC on EEG data elicited by picture encoding and at recall, we first filtered the epochs with the function 'eegfilt' from the EEGlab toolbox of Matlab.[51] Low frequencies (4 – 12 Hz) were filtered with a window of 0.3 times the frequency of interest, centred on each frequency step. Similarly, high frequencies (30 – 140 Hz) were filtered with a window of 0.7 times the frequency of interest. This allowed for better sensitivity and allowed Δ(hf) to be always higher than the maximum phase of coupling (low frequency + delta (LF)). Variable bandwidth of phase and amplitude has been shown to increase sensitivity reducing false negatives. It also maintains the equilibrium between the bandwidth of high frequencies needing to be higher than twice the central low frequency, to avoid biases toward slow-modulating rhythms.[52] Filtered data was z normalized to trial average to ensure that all observed effects were not driven by an Event-Related Potential (ERP). After filtering, we extracted the angle of the Hilbert transform of low frequencies and calculated the phase. High-frequency amplitudes were calculated by the square of the Hilbert envelope.

To quantify phase-amplitude coupling we calculated the mean amplitude of each high-frequency per low-frequency phase bin in 18 different bins of 20 degrees each (e.g., Tort et al.,[32] Pacheco Estefan et al.,[37] Staresina et al.,[53] and Heusser et al.[54]) for each trial of each patient. Each trial was then transformed into a probabilistic distribution (sum = 1) by dividing each bin by the sum of all bins. We then averaged the distributions over trials and calculated the Modulation Index (MI) using the Mean Vector Length (MVL) method,[31] which takes the absolute value of the mean complex vector of binned amplitudes to increase specificity towards unimodal phase-amplitude coupling. Similar results were obtained using the Kullback-Leibler Distance with Shannon's entropy approach as a measure of non-uniformity[21,32] However, we noted that this method could create a bias towards lower modulating frequencies by picking up on bimodal coupling events that originate from higher modulating phases. Therefore, the data reported in our study are the results obtained with the MVL approach. To create surrogate distributions, each amplitude trial was cut at a random timepoint –excluding the first and last 10% of timepoints - and the two obtained amplitude time series were permuted. The time-shuffled amplitude was then binned with its corresponding non-shuffled phase, hence leading to a random phase preference for each trial. The MVL of this

random distribution was then calculated in the same fashion as for the experimental trials. We repeated this procedure 1000 times and stored the MVL values of each iteration and participant. We then demeaned PAC data, both real and surrogates in order to perform t-scoring and statistical testing. To confirm that this normalization procedure did not affect the statistical structure of the data we performed a correlation test and observed a rho value of 1 between the original PAC data and the demeaned PAC data.

For statistical testing, we t-scored the real PAC across patients and identified clusters of contiguous pair of frequencies that showed to be significant at a threshold set to 2.5%. We repeated the process for each surrogate matrix and obtained a distribution of 1000 t-sums representing the maximum possible cluster in surrogate data. We only considered significant clusters in the empirical data whose summed t-values exceeded 95% of the surrogate distribution of t-sums.

Mean Opposition Vector Index (MOVI)

To test whether PAC for the memory encoding and memory recall periods rested on different phases of theta, we used an adaptation of the MVL approach described elsewhere[33] on the difference between two distributions of amplitude per phase bin. We denoted $Distrib_A$ and $Distrib_B$ two distributions of amplitude per phase bin. Distributions A and B were calculated in the following way: we denoted f_A and f_p as the frequencies for amplitude and phase respectively of one condition. Within the significant cluster of PAC of the said condition, we filtered data for each pair of frequencies as following the same procedure implemented to estimate PAC and created a binned distribution of mean amplitude per phase bin, averaged over trials. The distributions of each pair of frequencies were normalized to a probabilistic distribution (sum = 1) to avoid having different magnitudes of amplitude in function of the different frequencies. Once we had a distribution for each pair of frequencies, we averaged all the distributions across frequencies to obtain one single distribution with the average phase preference of the PAC cluster. The second distribution was obtained the same way but by extracting pairs of frequencies from the PAC cluster of its specific condition. In this way, we obtained 2 distributions of mean amplitude per phase bin A and B that each represented the mean amplitude per phase bin of their PAC cluster.

We then calculated MOVI as follows:

1- First, we calculated the difference between $Distrib_A$ and $Distrib_B$.
2- We added to this difference twice the mean of a uniform distribution with the same number of phase bins noted as: $2 * \frac{1}{nbins}$ to have only positive values that were similar to a probabilistic distribution (sum = 1). However, since the resultant distribution came from the difference between two distributions, if opposed, the difference between the peak and the through of this new distribution would have twice the magnitude of either of the original distributions A and B.
3- To correct for this issue, we divided the result by 2 to keep the magnitude of modulation of the alternative distribution $Distrib_{Diff}$ similar to the magnitude of the two distributions it compares.

The complete formula used to calculate the alternative distribution was:

$$Distrib_{Diff} = \frac{(Distrib_A - Distrib_B) + 2 * \frac{1}{nbins}}{2}$$

4- To avoid having false positives and greater effects due to the difference in two distributions, the resulting alternative distribution was normalized to a probabilistic distribution (sum = 1) by dividing each phase bin by the sum of all bins.
5- We calculated MOVI as the MVL of the resultant distribution $Distrib_{Diff}$ as follows:

$$MOVI = \left| \frac{\sum Amp_{bin} * e^{i\theta_{bin}}}{nbins} \right|$$

where Amp_{bin} is the amplitude of each phase bin and θ_{bin} is the angle of each phase bin and *nbins* is the number of phase bins and MOVI was the calculated MVL of this distribution. The basic premise of MOVI is that if two distributions are opposite, the alternative distribution will be a resulting one with higher MVL than either of the original distributions. If two distributions are in the same direction, then the resultant distribution should be flat and MOVI would be low. And, if one distribution has very low PAC in the surrogate trials, MOVI would be similar to the one obtained from the experimental (real) PAC, avoiding, therefore, finding false positives due to a one directional PAC amplitude in the data.

For the statistical analysis of MOVI, we averaged the experimental MOVI value across patients and the surrogate distributions over patients and then compared the 1000 surrogate scores with the experimental value using a z transformation of the experimental value, which was computed as the experimental MOVI value minus the mean of the surrogate MOVI values, over the standard deviation of the surrogate MOVI distribution ([z = (MOVexp - mean(MOVIsurr)/std(MOVIsurr)]). We obtained a p-value associated to the z value by identifying the fraction of surrogate MOVI values below the experimental MOVI value. We considered significant an experimental MOVI value that was greater than 95% of surrogate MOVI values. Surrogates for MOVI were computed independently for each dataset A or B by shuffling trial labels 1000 times.

We used MOVI instead of more traditional methods for measuring distribution distance[55–57] because we wanted our measure to be dependent on the PAC strength between frequency pairs, and to be sensitive enough to pick on amplitude-driven opposition in angle

preference. Other phase opposition indexes such as inter-trial coherence (ITC) or pairwise phase consistency (PPC) do not take into account PAC strength, as they rely on the unit normalization of vectors and might lead to phase opposition reports for frequency pairs where PAC is low or even absent, but with phase spuriously opposed. Furthermore, from a methodological point of view, methods such as ITC rely on the density of occurrences[56,58] that does not consider coupling strength of angle preference and where each trial is summarized into a single unit-normalized vector that does not take into account the overall distribution of amplitude per phase but rather only detects the peak, which may compromise the results (i.e., inflating type I and type II errors). Instead, MOVI is a measure that considers the average distribution across trials and that relies on common effects in terms of PAC and phase preference such as the Kullback-Leibler Distance (DKL) and the Jensen-Shannon Divergence (JSD), a symmetrical adaptation of the DKL,[55] thereby improving the sensitivity to study theta-gamma phase opposition in task designs like ours. In fact, similar results were obtained using the DKL approach. DKL has been commonly used to compute the modulation index during PAC with an adaptation of the Shannon entropy formula, comparing an experimental distribution to a uniform distribution. However, DKL is used to assess the difference between two distributions A and B with the following formula:

$$DKL(A|B) = A * \log\left(\frac{A}{B}\right)$$

To implement DKL in our data, we filtered and binned the data following the same procedure described in the MOVI subsection of the methods section of the main manuscript. However, we now directly compared the distributions without passing by an alternate distribution like in MOVI. The results using DKL replicated the ones described in the main paper using MOVI. More specifically, the use of DKL revealed significant gamma band activity coupling to opposed theta phase states during memory encoding and recall ($z = 3.48$, $p = 0.002$) and that theta-gamma PAC opposition was statistically significant for remembered episodes ($z = 2.97$, $p = 0.003$) but not for forgotten episodes ($z = 0.51$, $p = 0.27$). These results provide converging evidence of theta-gamma phase opposition using two distinct analytical approaches in our data.